THESIS FOR THE DEGREE OF LICENTIATE OF ENGINEERING

Electromechanical Behavior of Organic Mixed Ionic-Electronic Conductors

Judith Pons i Tarrés

CHALMERS

Department of Chemistry and Chemical Engineering

Division of Applied Chemistry

CHALMERS UNIVERSITY OF TECHNOLOGY

Göteborg, Sweden, 2025

Electromechanical Behavior of Organic Mixed Ionic-Electronic Conductors

Judith Pons i Tarrés

Thesis for the degree of Licentiate of Engineering

Nr. 2025:12

Department of Chemistry and Chemical Engineering
Division of Applied Chemistry
Chalmers University of Technology
SE-41296 Göteborg

Phone: +34 648 107 444

Cover:

Typical configuration of an organic electrochemical transistor

Chalmers Reproservice

Göteborg, Sweden, 2025

This project has received funding from the European Research Council (ERC) under grant agreement no. 101043417

Electromechanical Behavior of Organic Mixed Ionic-Electronic Conductors

ABSTRACT

Organic mixed ionic-electronic conductors (OMIECs) are a new class of organic materials that connect the hard, rigid world of traditional electronics with the soft, ion-conducting nature of biological systems. Because they can move both electronic and ionic charges, they are especially well suited for interacting with living tissues and have become important to the growing field of organic bioelectronics. A key device based on OMIECs is the organic electrochemical transistor (OECT), which has become the benchmark for evaluating material performance in applications ranging from biosensing to neuromorphic computing.

While the electrical properties of OMIECs are well known, their mechanical properties — and how these change during device operation — are still not fully understood and are essential for a stable, long-term integration with biological tissues without damage, such as tissue scarring. The electrochemical redox processes that come with OECT operation involve ion and solvent uptake, which can lead to swelling, plasticization, and microstructural changes that directly affect the material's mechanical properties.

This thesis aims to investigate the fundamental coupling between electrical and mechanical properties in OMIECs during electrochemical operation. OECTs are used as a model system to study ionic-electronic transport, while *in situ* techniques such as electrochemical nanoindentation (EC-NI) and electrochemical atomic force microscopy (EC-AFM) are applied to track changes in mechanical properties, concretely the elastic modulus. The work focuses on a thiophene based copolymer p(g_3TT-T2) (PTTEG) while also exploring how side chain design affects both electrical and mechanical behavior.

Overall, this work shows that OMIECs can be engineered so their mechanical properties are tunable, even stabilized, across redox cycles. By combining device physics, material characterization, and fabrication, this thesis offers a way to understand electromechanical coupling in OMIECs; insights that are key for designing future bioelectronic devices.

Keywords: organic mixed ionic-electronic conductors, organic electrochemical transistors, electrochemical doping, electrical and mechanical properties.

NOMENCLATURE

OMIECs	organic mixed ionic-electronic conductors
OECTs	organic electrochemical transistors
EC-NI	electrochemical nanoindentation
EC-AFM	electrochemical atomic force microscopy
C^*	volumetric capacitance
μ	charge carrier mobility
PEDOT:PSS	poly(3,4-ethylenedioxythiophene):poly(styrene sulfonate)
p(g2T-TT)	poly[2-(3,3'-bis(triethylene glycol monomethyl ether)-[2,2'-bithiophen]-5-yl)thieno[3,2-*b*]thiophene]
BBL	poly(benzimidazobenzophenanthroline)
NDI	naphthalenediimide
PTTEG	p(g_3TT-T2); poly[2-([2,2'-bithiophen]-5-yl)-3,6-bis(triethylene glycol monomethyl ether)thieno[3,2-*b*]thiophene]
V_{th}	voltage threshold
EGOFETs	electrolyte-gated organic field-effect transistors
OFETs	organic field-effect transistors
PDMS	polydimethylsiloxane
PBTTT	poly[2,5-bis(3-tetradecylthiophen-2-yl)thieno[3,2-*b*]thiophene]
CV	cyclic voltammetry
E_{ox}	oxidation potential
EG	ethylene glycol
EC	electrochemical
WE	working electrode
CE	counter electrode
RE	reference electrode
g_3TT	3,6-bis(triethylene glycol monomethyl ether)thieno[3,2-*b*]thiophene
g_m	transconductance
g_m^*	dimension-normalized transconductance
I_{on}/I_{off}	on/off-current ratio
I_{DS}	drain-source current

I_{GS}	gate-source current
V_{DS}	drain-source voltage
V_{GS}	gate-source voltage
w	channel width
d	channel thickness or active layer thickness
τ	response time
Pa-C	parylene-C
E	elastic modulus
Ag/AgCl	silver/silver chloride
Pt	platinum
EIS	electrochemical impedance spectroscopy
SSA	small signal analysis

PUBLICATIONS

This thesis consists of an extended summary of the following appended papers:

Paper I **Anomalous stiffening of a conjugated polymer during electrochemical oxidation**

Judith Pons i Tarrés, Di Zhu, Chiara Musumeci, Youngseok Kim, Dilara Meli, Hang Yu, Meghna Jha, Bryan D. Paulsen, Ruiheng Wu, Joost Kimpel, Zachary Laswick, Sri H. K. Paleti, Yadong Zhang, Stephen Barlow, Seth R.Marder, Jenny Nelson, Jonathan Rivnay, Christian Müller

Under review, **2025**

Paper II **Ambient Direct Arylation Synthesis of Thienothiophene Based Copolymers with Mixed Alkoxy and Oligoether Side Chains**

Di Zhu, Judith Pons i Tarrés, Joost Kimpel, Meghna Jha, Mariavittoria Craighero, Jesika Asatryan, Alberto Peinador, Zesheng Liu, Mats Fahlman, Jaime Martín, Alexander Giovannitti, Christian Müller

Manuscript in preparation, **2025**

The author has published the following papers which are not included in the thesis:

Paper III **Benchmarking the Elastic Modulus of Conjugated Polymers with Nanoindentation**

Sri Harish Kumar Paleti, Shuichi Haraguchi, Zhiqiang Cao, Mariavittoria Craighero, Joost Kimpel, Zijin Zeng, Przemyslaw Sowinski, Di Zhu, Judith Pons i Tarrés, Youngseok Kim, Qifan Li, Junda Huang, Alexei Kalaboukhov, Besira Mihiretie, Simone Fabiano, Xiaodan Gu, Christian Müller

Macromolecules, **2025**, 58, 3578-3588

Paper IV **Unravelling the operation of organic artificial neurons for neuromorphic bioelectronics**

Pietro Belleri, Judith Pons i Tarrés, Iain McCulloch, Paul W. M. Blom, Zsolt M. Kovács-Vajna, Paschalis Gkoupidenis, Fabrizio Torricelli

Nature Communications, **2024**, 15, 5350

CONTRIBUTION REPORT

Paper I	Main author. Conceived the study and wrote the manuscript. Carried out the EC-NI, part of the EC-AFM and e-QCMD, CV and stability measurements, as well as associated data analysis.
Paper II	Co-author. Fabricated the devices necessary for the study and measured their CVs and electrical and mechanical properties of the copolymers in the neat state and redox cycling. Help with the writing of those parts.

TABLE OF CONTENT

Chapter 1

Introduction

1.1 Organic bioelectronics

Over the past few decades, organic electronic materials have emerged as a transformative alternative to traditional inorganic semiconductors. While inorganic electronics, dominated by silicon, offer exceptional charge-carrier mobilities (electrons) and thermal stability, they are typically rigid, brittle, and planar.[1] These limitations have motivated the search for materials that can combine electronic functionality with mechanical and chemical compatibility with that of biological systems.

Organic materials offer several unique advantages in this context. Their naturally low stiffness makes them flexible and stretchable, allowing devices to conform to curved or moving surfaces without compromising performance. They can also be processed from solution, enabling scalable and relatively low cost fabrication, and their properties can be tuned via chemical synthesis to optimize both electrical and mechanical characteristics for specific applications.[2]

Many biological processes require the presence and interaction of ions and electrons, e.g., enzymes holding ions or electron transport in photosynthesis. Hence, efficient bioelectronic devices benefit from recognizing both ionic and electronic charge carriers. Organic mixed ionic-electronic conductors (OMIECs) combine electronic conduction, through a π-conjugated backbone, with the ability to absorb and transport ions from biological or aqueous environments, using polar pendent groups, with plenty opportunity for tunability.[3] One popular bioelectronic device is the organic electrochemical transistor (OECT), which has been used in applications ranging from biosensors to neuromorphic computing and, more importantly in this work, are widely employed for the characterization of organic mixed ionic-electronic conductors (OMIECs), which constitute the channel material.[4, 5]

These attributes have driven the development of organic bioelectronics, an interdisciplinary field that comprises the design and application of devices that record, stimulate, or modulate biological activity through the transduction of ionic and electronic signals. For example, neural interfaces for recording and stimulation, platforms for monitoring electrophysiological signals, implantable stimulators for therapies, e.g., vagus nerve modulation or cardiac pacing, wearable health monitors, and biosensors for detecting metabolites such as glucose and lactate. A major advantage of OMIECs in an OECT device is their ability to operate at low voltages, which lowers the risk of electrochemical damage to delicate tissue while still delivering sensitive and stable signals.[6-8]

Despite their promise, organic bioelectronic materials face several challenges that continue to motivate research in the field. Long term operational stability in aqueous environments remains a concern, as does performance reproducibility and the development of scalable, industrially relevant fabrication processes.[9]

1.2 Aim and scope

This thesis explores the coupling between electrical and mechanical properties in a hole-transporting OMIEC, with a focus on how these properties evolve during electrochemical doping and dedoping. Understanding how mechanical properties change with the electrochemical state of the polymer is essential for predicting device behavior. To address this, OMIEC films are characterized *in situ*, using techniques capable of probing mechanical properties during electrical operation, including electrochemical nanoindentation (EC-NI) and electrochemical atomic force microscopy (EC-AFM) **(Paper I).** Organic electrochemical transistors (OECTs) are employed as a model platform, combining steady-state and transient techniques (small signal analysis) allowing to reliably extract key figures of merit like $[\mu C^*]$ **(Paper II)**. These measurements are correlated with electrical performance parameters extracted from OECT operation to establish direct relationships between ionic-electronic transport and mechanical response. The scope of the work further includes all the fundamentals about OECTs as well as its fabrication procedure, while also seeking to provide a comprehensive understanding of the electromechanical coupling in OMIECs.

Chapter 2

Organic mixed ionic-electronic conductors – electrical properties

2.1 Organic mixed ionic-electronic conductors

Some conjugated polymers, small molecules and radical polymers can act as organic mixed ionic-electronic conductors (OMIECs).[4, 10, 11] OMIECs can conduct both ionic and electronic charge carriers, allowing operation in a wide range of devices, including OECTs, biosensors, and soft actuators.[3] The ionic carriers populating OMIECs can be extrinsic (i.e. sourced from an electrolyte in contact with the material) or intrinsic (i.e. from component polyelectrolytes), e.g., PEDOT:PSS (a conjugated polyelectrolyte complex in which the polyanion PSS provides fixed anionic sites that facilitate ion exchange and swelling, while PEDOT offers high electronic conductivity, which is synthesized in its oxidized state). To become conductive most OMIEC films require electrochemical doping – the oxidation or reduction of a semiconductor via electron transfer to or from a working electrode – and the charge neutrality is maintained by the electrolyte counterions (an opposite polarity ion migrating into the film), allowing the formation of polarons, i.e. radical cations or anions on the polymer backbone.

Unlike traditional organic semiconductors, which rely solely on electronic conduction, OMIECs are engineered to also accommodate ion motion within their bulk, enabling volumetric doping and dedoping processes – a fundamental process in bioelectronics, wearable electronics, energy harvesting and energy storage.[3, 9]

OMIECs can be designed from conjugated polymers to have different electronic characters: (1) p-type backbones that conduct holes, e.g. PEDOT:PSS, p(g2T-TT) (Figure 1a),[12] (2) n-type backbones that transport electrons, e.g. BBL and NDI-based polymers,[13] (Figure 1b) and (3) ambipolar systems which can transport both carrier types, such as DPP-based copolymers.[14] In p-type OMIECs, hole accumulation on the backbone is compensated by anions from the electrolyte migrating into the polymer film while in n-type OMIECs, injected electrons are stabilized by cations penetrating the film. Ambipolar OMIECs can support both processes, with anions and cations moving selectively depending on whether the material is hole or electron doped. This reflects the necessity of ionic exchange to maintain charge neutrality during redox cycling (doping and dedoping).

Ionic transport happens when mobile ions from an electrolyte penetrate the OMIEC film through diffusion (passive) or migration (driven by potential gradients). This transport occurs through hydrophilic domains, commonly polar polymer sections or side chains, allowing accommodation of ions and their hydration shells. In electronic transport holes and/or electrons move through a percolated network of conjugated polymer via delocalized π-orbitals in the backbone (intra-chain) or through π-π stacks between chains (inter-chain). Ion-electron/hole coupling happens volumetrically, using the entirety of the active materials, with the number of couplings between ions and charges resulting in a potential-dependent volumetric capacitance (C^*, being the number of charges induced per unit voltage per mass). This coupling governs key properties such as conductivity, volumetric capacitance, and electrochemical switching, which are important for many device applications.[15] OMIEC materials can be homogenous, i.e. a single component transporting both ionic and electronic charge, or inherently heterogenous, such as block copolymers or blends of distinct ionic and electronic transporting components.

2.1.1 OMIEC design

The design of OMIECs is based on the need to accommodate and stabilize ionic and electronic charges during transport, while making sure that ionic conduction modulates electronic charge density within the conjugated backbone. An immediate problem of OMIECs is that the aromatic core is hydrophobic. Hence, the addition of side chains with polar parts helps with efficient ion uptake and mobility, while the conjugated backbone provides pathways for electronic conduction via delocalized π-electrons – backbone planarization is linked to better conduction which can be achieved with, e.g., larger aromatic systems but those can lead to solubility issues. This is where the strategy of a rigid backbone with flexible and hydrophilic side chains emerged. Side chains help with solubility, to process the material, to get certain mechanical properties and have a profound impact on how the material organizes.

Conjugated polyelectrolyte complexes emerged as an early strategy to combine ionic and electronic conduction, achieved by incorporating ionic groups onto the polymer backbone; the most well-known example is PEDOT:PSS. This design enables intrinsic ionic functionality but also comes with limitations: immobile ionic sites can lead to reduced electronic mobility and excessive swelling in aqueous environments, sparking efforts to search for alternative strategies such as the addition of hydrophilic, but neutral, side chains like ethylene glycol (EG).

EG side chains allow dynamic and reversible ion penetration into the polymer and decouple the ionic transport functionality from the electronic backbone. A well-known example is p(g2T-TT).[12] EG side chains enhance ion solvation and transport, leading to higher volumetric capacitance – promoting electrochemical doping. They also improve compatibility with bioelectronic environments and are synthetically tunable upon adjusting chain length, density of incorporation, and distribution to optimize swelling and ionic uptake. Despite their strengths, EG side chains face some challenges: strong hydrophilicity that leads to excessive amount of swelling upon electrolyte uptake leading to changes in microstructure, possible degradation and a slower device response. In contrast, alkyl side chains are hydrophobic which can help reduce swelling and as a result improve film stability and microstructural order,[15] often enhancing backbone packing and electronic mobility, e.g. PBTTT. However, they are nonpolar and cannot coordinate or solvate ions, which limits ionic conduction and reduces volumetric capacitance.[3] To balance those competing effects, mixed side chains emerged where both glycol and alkyl or alkoxy units are incorporated into the same polymer. EG units provide ionic accessibility, while alkoxy units suppress over-swelling and preserve the microstructure - leading to improved performance in devices such as OECTs. An example the copolymers used in **Paper II** and [16].

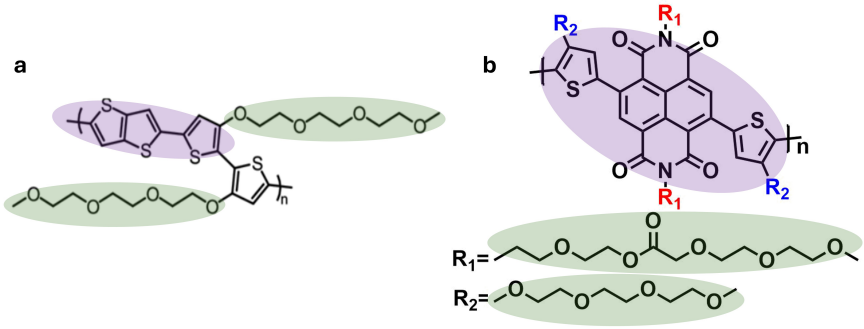

Figure 1. Chemical structures of (a) p-type (p(g2T-TT)), (b) n-type (p(gNDI-g2T)). Highlighted in green: side chains responsible for ion transport. Highlighted in purple: π-conjugated backbone, responsible for charge transport (electrons/holes).

2.1.2 Device applications

OMIECs have emerged as versatile materials for a broad range of technologies where the coupling of ionic and electronic transport is central to device function. OECTs have received significant attention to benchmark OMIECs properties, measuring some basic properties such as $\mu$and C^*(electronic carrier mobility and volumetric capacitance, respectively). Their product is a figure of merit in OECTs and it is correlated to the transconductance, g_m, a measure of amplification. Other applications range from battery electrodes to electrochromic windows and sensors,[4, 6, 17-21] where their application-properties relations can be found below:

Device	Figure(s) of merit	OMEIC property
OECT	Transconductance Switching speed Operating window	μ, C^* transit time, $\sigma_{ion/electron}$ $V_{th.}, E_{redox}$
Batteries	Specific capacity Energy density Switching speed Operating window	C' E_{redox}Transit time, σ_{ion} E_{redox}
Electrochromic	Coloration efficiency Switching speed Operating window	Band gap, $\sigma_{ion/electron}$ Transit time, $\sigma_{ion/electron}$ V_{th} , E_{redox}
Actuators and artificial muscles	Strain/stress output Response time Cycle stability	Ion uptake and swelling capacity Ionic mobility and diffusion Mechanical modulus and redox reversibility
Neuromorphic devices	Synaptic weight modulation/retention time Plasticity (STP/LTP) Energy per spike	Ion diffusion and redox kinetics Dynamic ion-electron coupling and device hysteresis C^*, σ_{ion} and charge injection efficiency

Table 1. OMIECs application-properties relations.

2.2 OECTs

Transistors are fundamental building blocks of modern electronics, serving as switchers and amplifiers; switching current flow on or off (enabling digital logic) and as amplifiers, they translate small input signals to larger outputs. These two functionalities lead to applications in a wide range of electronic systems, from microprocessors to biological signal amplifiers.[5] Conventional transistors are fabricated from inorganic semiconductors – silicon being the most well-known material; they dominate the digital electronics industry thanks to their speed, stability, and scalability.[22] However, their rigid nature limits their integration with soft, flexible, and biological systems. Organic transistors offer the possibility to extend transistors into new fields where high performance is not the main goal but rather biocompatibility and ion to electron transduction. Since they are built from π-conjugated polymers or small molecules, they can be processed from solution, printed, or deposited on flexible substrates[23] and can also be chemically engineered to introduce functionalities that are not possible in silicon, such as ion permeability, biocompatibility and mechanical softness.[9]

The common organic transistors are: OFETs (organic field-effect transistors), EGOFETs (electrolyte-gated organic field-effect transistors) and OECTs (organic electrochemical transistors) (Figure 2). OFETs have a current modulation at the interface between the semiconductor and the dielectric, without ion penetration into the bulk. Contrary, in EGOFETs, an electrolyte replaces the dielectric so that ions can accumulate at the interface between the electrolyte and the semiconductor (becoming an interfacial double layer). In OECTs this is taken one step further: those ions penetrate into the semiconductor, taking place in the bulk of the material and not just at the interface (volumetric doping); the entire volume of the semiconductor changes its conductivity.[5] This property does not only make OECTs attractive for applications in bioelectronics and soft systems but also ideal model devices for probing and quantifying OMIEC performance.

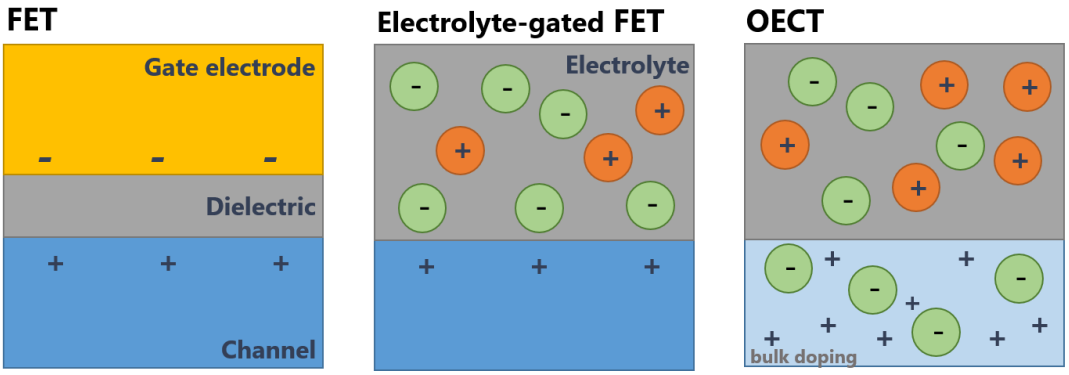

Figure 2. Type of Organic Transistors: (a) Field-effect transistor (FET) with accumulation of mobile electronic charges near the channel-dielectric, (b) electrolyte-gated field-effect transistor (EGOFET) where a double layer capacitor is formed at the channel-electrolyte interface, (c) organic electrochemical transistor (OECT) where ions penetrate the semiconductor, leading to changes through the whole volume of the film (volumetric capacitance), where the same voltage induces more electronic charge in the channel.[5]

2.2.1 Working principle

An OECT is a three-terminal device: the source, the drain, and the gate electrodes. It uses an OMIEC as the active channel material which connects the source and the drain. The OMIEC is surrounded by the electrolyte – either in a liquid form or solid-state ionic conductor –typically held in place by a polydimethylsiloxane (PDMS) or glass reservoir (Figure 3a). The gate electrode can be placed in different ways, the most common being suspended into the solution (out-of-plane, configuration suitable for benchtop experiments) and acts as the medium, transmitting ionic signals from the gate to the channel. By doing so, it enables electrochemical doping (introduction of charge carriers, accumulation-mode OECT) or dedoping (removal of charge carriers, depletion-mode OECT) of the OMIEC (Figure 3b), drastically changing its electronic conductivity.

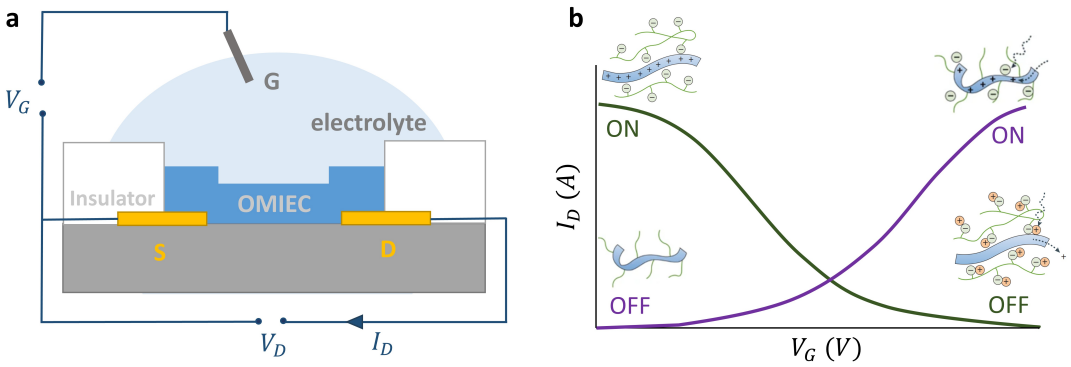

Figure 3. (a) Typical structure of an organic electrochemical transistor (OECT), showing the source (S), drain (D), insulator, OMIEC, electrolyte and gate (G), (b) transfer curves of depletion (green) and accumulation (purple) mode OECTs. Upon application of a gate voltage in depletion mode, the holes are replaced by cations and the transistor turns OFF while in the accumulation-mode holes accumulate and compensate anions, turning the transistor ON. Figures adapted from [5].

The gate voltage (V_G) modulates the injection of ions into the channel (redox state or doping level) while the drain current (I_D) induces a current proportional to the amount of holes or electrons in the channel (probing the doping level). The input (V_G) controls the output (I_D) and large modulation in the drain current can be achieved for low gate voltages (described by transfer curves; Figure 4a) owing to the volumetric doping, making OECTs efficient switches and powerful amplifiers.[24, 25] The steeper the transfer curves, the larger the amplification, also known as transconductance (g_m), which is the first derivative of the transfer curve: $g_m = \frac{\partial I_D}{\partial V_G}$ a figure of merit of OECTs (Figure 4a). Since volumetric doping occurs, the thickness is directly proportional to the transconductance (g_m) but inversely proportional to the response time (τ) (Figure 4b). This is because the volume becomes larger and as a result it takes longer to charge (reach steady state). Below the kHz range, the transconductance of OECTs is much larger than field effect transistors of the same dimensions, which is the speed where most biological events take place. However, at higher frequencies the OECT will not be able to respond since its amplification will drop out rapidly (Figure 4c).

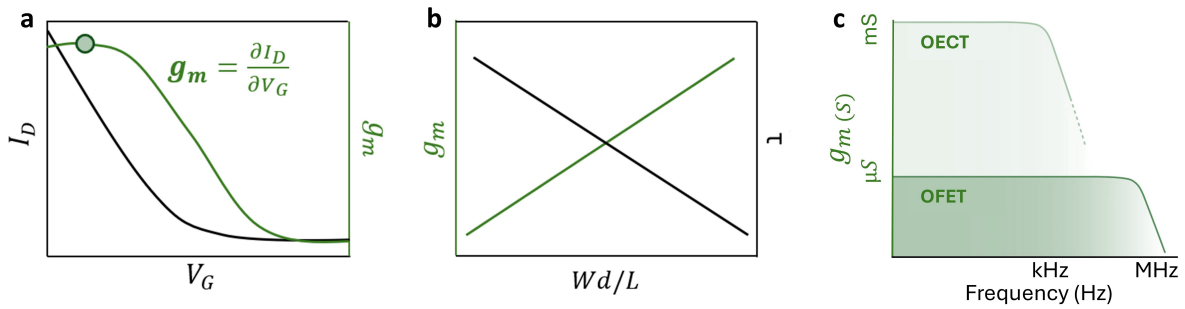

Figure 4. (a) Transconductance and response time depending on the OECT channel dimensions which are directly proportional to g_m but inversely proportional to τ, (b) transfer curve of an OECT working in accumulation mode (black) and how to obtain the g_m. $g_{m,max}$ (green dot) is reported as one of the steady-state figures of merit of an OECT, (c) transconductance comparison between electrochemical and organic field effect transistors depending on the frequency. (c) obtained from [5].

2.2.2 Bernards-Malliaras model

The first analytical model of OECT operation was introduced by Bernards and Malliaras in 2007 and assumes that ions from the electrolyte enter the channel and change the electronic conductivity through its volume, capturing steady-state conditions. According to this model, OECTs are not treated as a single electronic transistor but as the combination of two coupled circuits: an ionic circuit and the electronic circuit (Figure 5).[27]

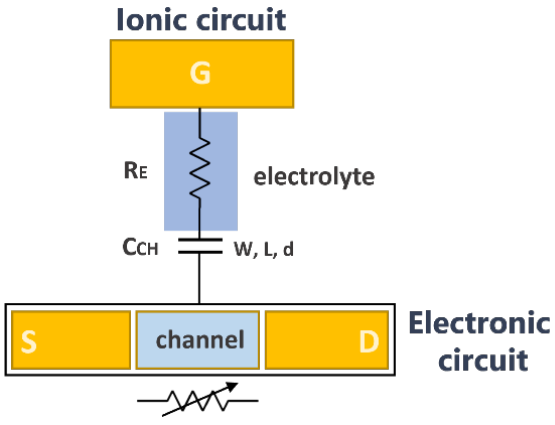

Figure 5. Bernards-Malliaras model which separates the OECT into two circuits: the ionic and the electronic. Figure adapted from [27]

The ionic circuit describes the flow of ions in the gate-electrolyte-channel structure, and it can be understood as an electrochemical capacitor. When a V_G is applied, ions from the electrolyte migrate into or out of the OMIEC channel, depending on the polarity of the bias. This ion conduction leads to electrochemical doping or dedoping of the material. As a result, this circuit can be represented as a resistor (describing the flow of ions in the electrolyte) in series with a capacitor (describing the storage of ions on the channel) which can be referred to as an RC circuit (Figure 5). This model implies a purely capacitive process; ions injected in the channel do not exchange charge with the organic film but rather electrostatically compensate the presence of opposite charges.[28]

The electronic circuit describes the flow of electronic charge in the source-channel-drain structure according to Ohm's law where injected ions replace electronic carriers. It is treated as a variable resistor, in which the electronic charge drifts under the influence of the local potential. In the presence of ions from the electrolyte, the channel undergoes redox reactions, resulting in changes in its conductivity. The electronic circuit utilizes these conductivity changes to modulate the flow of electrons and when a voltage is applied between the source and drain electrodes (V_D), electronic current flows through the channel. The modulation of the OMIEC conductivity, induced by the ions in the ionic circuit, affects the magnitude of the electronic current. This modulation can be controlled by the V_G applied to the OECT, which further influences the electronic circuit's behavior.[27]

2.2.3 OECT characterization techniques

A widely used method for the determination of the electronic carrier mobility (the velocity of charged carriers upon electric field), μ, and the volumetric capacitance (capacitance of the channel per unit volume), C^*, involves two methods: (1) OECT characterization (transfer curves) and (2) electrochemical impedance spectroscopy (EIS). From (1) we can extract g_m and then μC^* from Equation 1 or 2 while for (2) C^* can be obtained from EIS and as a result, μ is obtained by dividing $\frac{\mu C^*}{C^*}$.

The product μC^* describes the mixed ionic-electronic transport properties by telling of the efficiency of electronic transport and ionic charge storage.[4] Both metrics are related by Equation 1 for p-type OECTs, and Equation 2 for n-type OECTs, both operated at saturation:[27]

$$g_m = \frac{Wd}{L}\mu C^*(V_{th} - V_G) = \frac{\partial I_D}{\partial V_G} \quad (1)$$

$$g_m = \frac{Wd}{L}\mu C^*(V_G - V_{th}) = \frac{\partial I_D}{\partial V_G} \quad (2)$$

where, W, d, and L are the width, thickness and length of the OECT channel, respectively. V_{th} is the threshold voltage and V_G the gate voltage. This equation is derived from the transconductance of FETs, with the main difference being the terms that are governed by the volume of the active layer (d and C^*).[4] According to this equation, g_m is device geometry dependent, thus, it is best normalized against these when comparing the steady-state performance of different devices (g_m^*). The V_{th} can be determined by plotting the square root of the I_D as a function of V_G. The linear portion of the slope with the maximum magnitude is extrapolated, and the intersection with the x-axis gives the V_{th}.[29]

To apply the previous equations, it is required to be in the saturation regime. Hence, performing an output curve (I_D versus V_D across a range of V_G) is needed to determine which V_D needed to reach saturation depending on the V_G applied (Figure 6).

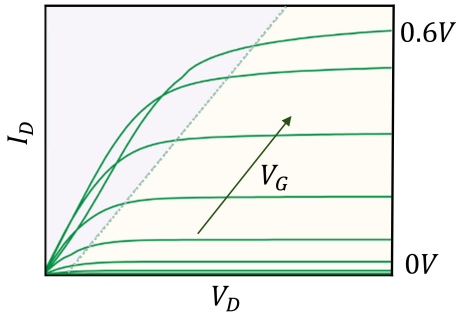

Figure 6. Output curves. I_D versus V_D across a range of V_G, to determine which V_D needs to be applied to be in the desired region: the linear region (grey) and the saturation region (beige) separated by a dotted green line.

In these measurements, the mobility is dependent on the voltage, as well as parasitic resistances included in the response and limited charge transport at low doping levels.[30, 31] The use of two different characterization methods for the determination of μC^* and C^* introduces uncertainty in the calculated mobility due to the propagation of errors. In addition, the OECT active layer typically swells during operation due to the uptake of hydrated ions, and as a result the *in operando* thickness varies from measured during a separate experiment, causing more inaccuracies.

2.2.3.1 Small signal analysis

The product μC^* is often used to benchmark OMIECs, but techniques to determine the two parameters independently are lacking which leads to ambiguities when comparing materials.[32] In this method, a small alternating current signal (of typically 10 Hz) is imposed on the voltage sweep, and the steady-state and transient response are acquired simultaneously. A constant V_D is applied, a voltage sweep $V_{G,DC}$ (slow triangular DC) is the steady-state response and the small signal $V_{G,AC}$ is the transient response (Figure 7).

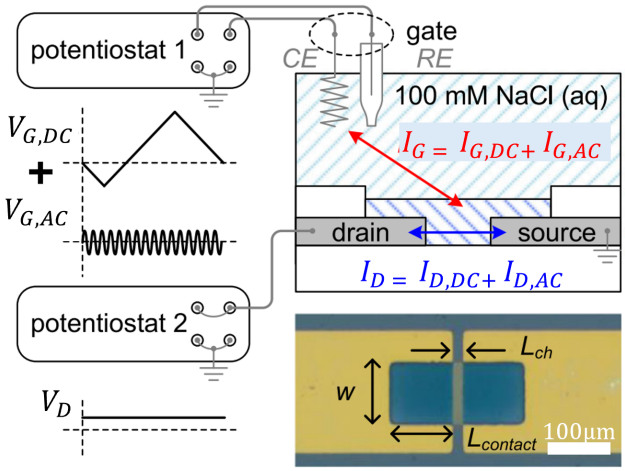

Figure 7. Device and measurement scheme for small signal analysis. A gate potential V_G consisting of a triangular potential $V_{G,DC}$ and a small-amplitude sinusoidal potential $V_{G,AC}$ is applied to the 100 mM NaCl aqueous electrolyte via a three-electrode configuration with a counter (CE) and a reference electrodes (RE), with a constant V_D. The lower inset depicts an optical microscopy image of the channel region of an OECT device. Figure extracted from [33].

By performing a Fourier transform analysis of these signals, the AC components of the gate and drain currents are separated into their real and imaginary parts. The imaginary (out-of-phase) component of the gate current corresponds to capacitive, non-Faradaic charging of the polymer, from which the volumetric capacitance C^* is obtained (Equation 3). The $I_{D,AC}$ reflects how this ionic charging modulates the electronic channel, and comparing the amplitudes and phases of the gate and drain responses yields the electronic transit time τ_e. From τ_e, μ is determined independently of the film thickness (Equation 4). Besides μ and C^*, small signal analysis of OECTs also provides information about a wide range of other parameters including

the transconductance, conductance $G = \frac{I_{D,DC}}{V_{D,DC}}$ and conductivity, σ, by normalizing G by $\frac{Wd}{L}$ through a single measurement.[33]

$$C^* = \frac{\Delta I''_{G,AC}}{2\pi f_{AC} \Delta V_{G,AC} \cdot vol} \tag{3}$$

$$\mu = \frac{L_{ch}^2}{\tau_e V_D} \tag{4}$$

where, $\Delta I''_{G,AC}$ is the amplitude of the imaginary part of the AC gate current, $\Delta V_{G,AC}$ is the amplitude of the AC gate voltage, f is the frequency, vol = wd · $(L_{ch} + L_{contact})$ is the volume of the active layer, L_{ch} is the length of the channel, τ_e is the electronic transit and V_D the drain voltage.

Unlike the EIS, small signal analysis is conducted with one frequency value, so that the parasitic response is superimposed onto the current value. While μ is barely affected by it, C^* decreases with increasing frequency and is typically underestimated for the typically used 10Hz AC frequency.[33] The accuracy of the method has been studied for 40 devices and different type of OMIECs (p-type, n-type and ambipolar) and shows that μ values have a lower $SD = 4\%$ than values from conventional methods $SD \approx 9\%$.[33]

Some of the main advantages compared to the conventional transfer curve and EIS for parameters extraction are the just mentioned lower SD for μ values, the independency of this one from the thickness, obtaining all parameters from a single measurement and the vector analysis (fourier) reduces the bias from parasitic effects that can inflate C^* or distort the g_m.

2.2.4 OECTs fabrication

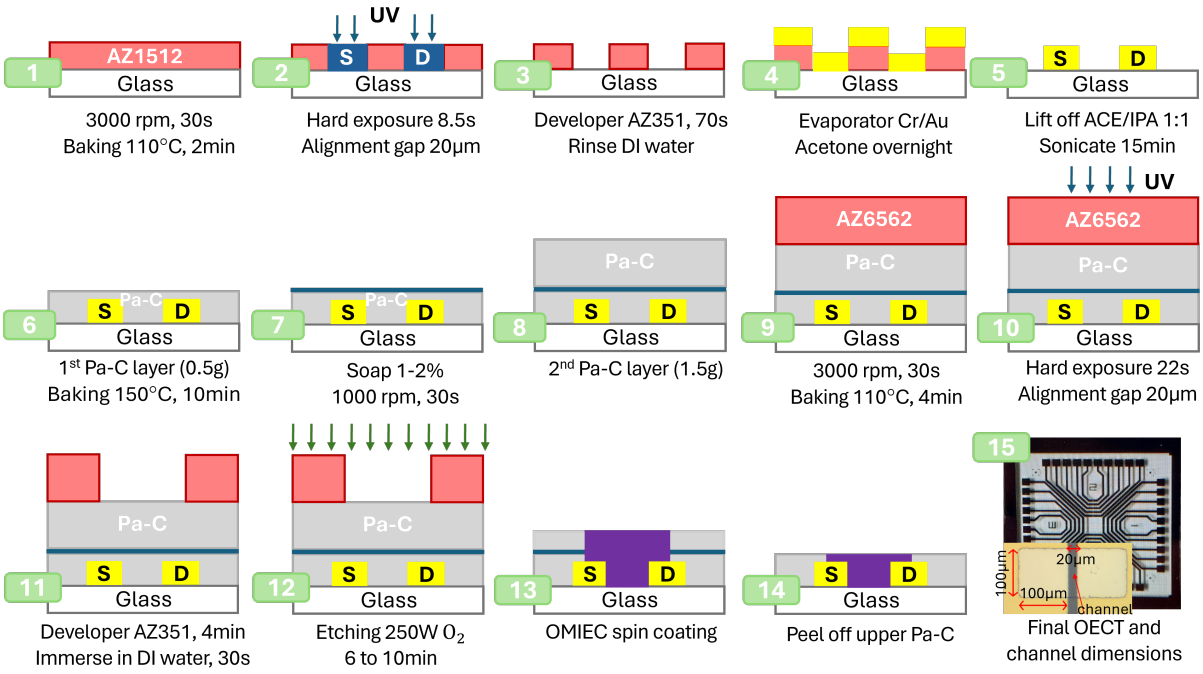

Figure 8. OECTs steps by step fabrication protocol

Steo-by-step guide for fabrication of OECTs after designing fabrication mask:

0. Glass slide cleaning process:

   a) Sonicate the glass slides in soap solution with DI water for 15 min
   b) Sonicate the glass slides in acetone/isopropanol (1:1) for 15 min and rinse with isopropanol and dry the glass slides with a nitrogen gun.

1. First photoresist deposition by spin coating and baking step:

   a) Place the glass slide on a spin-coater.
   b) Deposit a small amount of the photoresist (AZ1512) (sufficient to cover about ¾ of the glass slide) on the glass slide with a pipette.
   c) Spin the sample at 3000 rpm for 30 s.
   d) Put the glass slide on a hot plate at 110 °C for 2 min.

2. First UV Photolithography step (Karl Suss MA6 contact aligner):

   a) Set exposure time to 8.5 s, alignment gap to 20 µm and exposure type to hard and expose the glass slide.

3. Development in AZ351 developer:

   a) Prepare the developer bath 3:1 DI water:developer.
   b) Immerse the coated glass slides in the bath for 70 s.
   c) Rinse glass slides with DI water and dry with a nitrogen gun.

4. Metal evaporation step (Kurt J Lesker PVD e-beam evaporator):

a) Deposit a chromium film (50 Å Cr) on the glass slides to promote gold adhesion to the substrate.
b) Deposit gold on top (450 Å Au).
c) Leave immersed in acetone at least 4 hours (ideally overnight).

5. Lift off:

a) Change the solution to acetone/isopropanol (1:1)and sonicate for 15 min.
b) If required, use a Q-tip or a small brush soaked in acetone to remove the remaining undesired gold
c) Rinse with acetone and dry with nitrogen gun.

6. 7. 8. Parylene - C deposition step (CVD – Parylene coater):

a) For the first layer 0.5 g of Pa-C is coated in the substrate.
b) Bake the substrate at 150 °C for 10 min.
c) Place the glass slide on a spin-coater.
d) Deposit soap (1-2%, anti-adhesive promoter) on the glass slide using a pipette.
e) Spin the sample at 1000 rpm for 30 s.
f) 1.5 g are used for the second layer (1μm thick).

9. Second photoresist deposition by spin coating and baking step:

a) Place the sample on a spin-coater.
b) Deposit a small amount of the photoresist (AZ6562) (sufficient to cover about ¾ of the glass slide) on the glass slide with a pipette.
c) Spin the sample at 3000 rpm for 30 s and place it on a hot plate at 110°C for 4 min.

10. Second UV Photolithography step (Karl Suss MA6 contact aligner):

a) Set exposure time to 22 s, keep alignment gap to and exposure type to hard and expose.

11. Development in AZ351 developer:

a) Prepare the developer bath 3:1 DI water:developer.
b) Immerse the coated glass slides in the bath for 4 min.
c) Immerse the glass slides in DI water for 30 sand dry with a nitrogen gun.

12. Plasma etching step (Dry etch RIE - Plasma-Therm)

a) Apply O_2 plasma, power 250 W for 6 to 10 min until device channels are etched perfectly (check with microscope).

13. OMIEC spin-coating

a) Sample dependent. For 7-8 mg/mL PTTEG solution in chloroform, 50μL, 1500rpm and 1min are used as spin-coating parameters.

14. Peel off Pa-C

a) Peel off the Pa-C layer with the help of Sellotape tape, without touching the channels.

15. Device inspection with the microscope and ready to be measured.

2.2.5 OECT applications

Organic electrochemical transistors (OECTs) have gained attention in the field of bioelectronics for volumetric doping and high transconductance at low voltages (V < 1 V). In bioelectronics, OECTs enable high signal-to-noise electrophysiological recordings from tissues such as brain, as well as cutaneous measurements like electrocardiograms, owing to their local amplification and direct ionic/electronic coupling with biological fluids.[26, 34-37] Beyond recording, they can stimulate neurons, monitor cell cultures, and assess barrier formation or cellular health.[19, 38-42] As transducers in biosensors, OECTs detect electrolytes and metabolites such as glucose, lactate, and dopamine with high sensitivity and selectivity, and their integration with textiles and microfluidics has opened opportunities for wearable and multi analyte platforms.[43-47] Their high transconductance and low voltage operation also make them suitable for analog and logic circuits, where they have been employed in displays, logic gates, amplifiers, and flexible circuit architectures.[48-51] Finally, OECTs are promising building blocks for memory and neuromorphic devices, where ionic modulation of the channel enables short and long term plasticity, low power synaptic operation, and advanced architectures mimicking brain like computation.[6, 52-54] Collectively, these applications point out the application of OECTs and their potential as a bridge between electronics and biology.

2.3 PTTEG and copolymers

Here we studied the electrical properties of a thiophene based copolymer p(g_3TT-T2) (PTTEG) (Figure 9a) upon electrochemical doping. Firstly, we characterized p(g_3TT-T2) films with cyclic voltammetry and its stability upon 75 cycles which were recorded during repeated cycling between –0.4 V and +0.6 V *vs*. Ag/AgCl where the polymer is completely reduced and highly oxidized, resulting in voltammograms with the same shape indicating that the polymer can be reversibly reduced/oxidized (Figure 9b) and revealing an oxidation onset potential E_{ox} = +0.05V *vs*. Ag/AgCl. Secondly, SSA was performed on PTTEG to obtain different parameters, the μC^* figure of merit included (Figure 9c) with a $C^* \approx 180$ F cm^{-3}, $\mu \approx 2$ cm^2 V^{-1} s^{-1}.

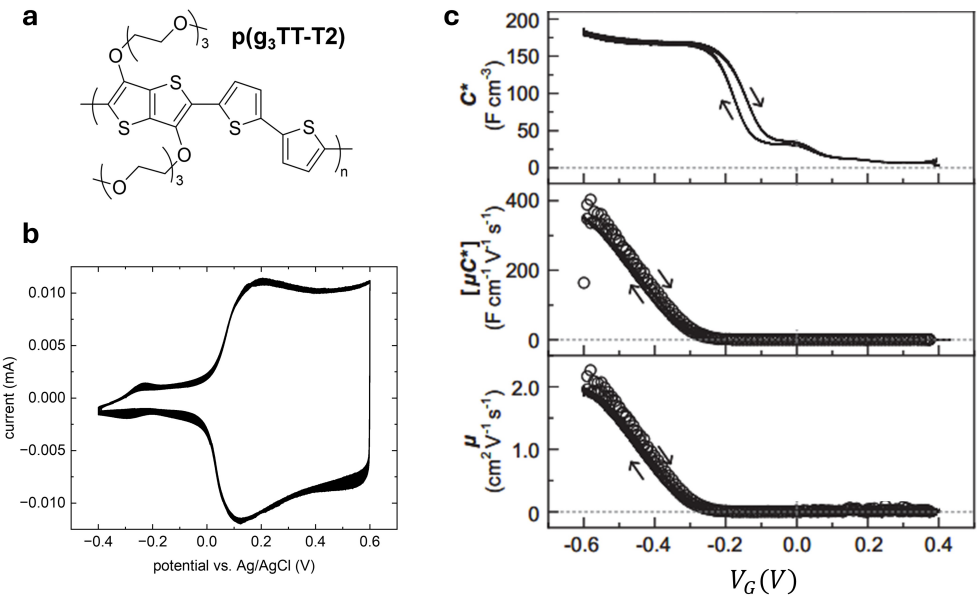

Figure 9. (a) Chemical structure of p(g_3TT-T2), (b) voltammograms recorded during repeated cycling up to 75 times at a scan rate of 10 mV s^{-1} using 0.1 M NaCl aqueous electrolyte, an Ag/AgCl RE and a Pt CE. (c) μ, C^* and μC^* values extracted using small signal analysis.

The same experiments were performed for the copolymers consisting of the same repeat unit with differing alkoxy and glycol side chains from **Paper II** (Figure 10 and Table 3): P12, P35, P59, P79 and P97, where the number represents the percentage of alkoxy side chains, e.g., P12 means 12 % alkoxy side chains and 88 % glycol side chains). However, for P79 and P97 small signal analysis was not successful since P97 was not conductive during CV measurements (Figure 10) and for P79 the OECT remained in the OFF state. This is tentatively attributed to their high apolar alkoxy side chain content, which limits ionic conduction, and hence withholds easy oxidation of the film contrary to the polymers with more glycol content.

Polymer	$E_{ox,onset}^{CV}$ (*V* vs Ag/AgCl)	μ_{max} ($cm^2\ V^{-1}\ s^{-1}$)	C^*_{max} ($F\ cm^2\ V^{-1}\ s^{-1}$)	$[\mu C^*]_{max}$ ($F\ cm^2\ V^{-1}\ s^{-1}$)
P12	0.22	2.9 ± 0.5	414 ± 12	1195 ± 184
P35	0.32	2.9 ± 0.3	357 ± 33	1031 ± 148
P59	0.42	2.2 ± 0.4	33 ± 4	72 ± 19

Table 3. Parameters extracted from cyclic voltammetry and small signal analysis.

The oxidation onset potential increases with increasing alkoxy side chain content (Figure 10 and Table 3). This can be attributed to the increased amount of hydrophobic side chain content in the polymer, hindering ion mobility and hence limiting the charge compensation from the ions in the electrolyte to stabilize the hole formation. Despite the increase in oxidation onset potential from P12 to P35 from 0.22 V to 0.32 V, the values for μ_{max} and C^*_{max} are comparable, leading to state-of-the-art $[\mu C^*]_{max}$ values over 1000 F cm^2 V^{-1} s^{-1} for both polymers. This is significantly higher than the values for PTTEG (P0) and P59, which are 360 and 72 F cm^2 V^{-1} s^{-1}, respectively. The lower figure-of-merit for PTTEG is tentatively assigned to its lower molecular weight than that of the polymers in the PX series, which all have a comparable molecular weight. It should be noted that $[\mu C^*]_{max}$ of P12 and P35 are reached at the highest potential of –0.6 V. This can be explained by the proportionality of μ, but, interestingly, the maximum C^* for both is reached after ca. 0.15 V after onset of capacitive

behavior. For P59, which is already expected to have poorer capacitive behavior due to high alkoxy side chain content, this is close to the end of the voltage sweep. Interestingly, the mobility of P59 reaches comparable values to P12 and P35, indicating the poor capacitance is detrimental to its figure-of-merit. Still, more research is required to understand the unexpectedly high C^* of P12 and P35.

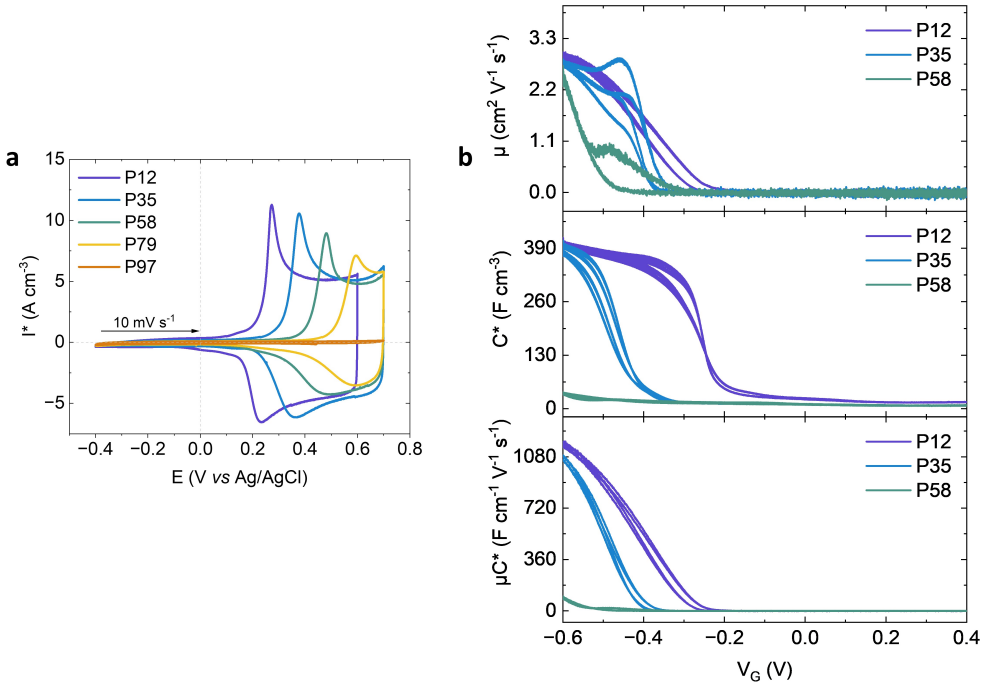

Figure 10. (a) cyclic voltammetry of the alkoxy-glycol copolymer series (b) and one forward and backwards scan as an example of the μ and C^* channel values extracted from small signal analysis.

Chapter 3

Organic mixed ionic-electronic conductors – mechanical properties

OMIECs are active materials and their electrical and mechanical properties evolve during operation. Even though the changes in electrical properties are well understood, much less is known about their mechanical response during electrochemical doping. In this context, the elastic modulus – a measure of how stiff a material is – is a key parameter. The changes in stiffness that occur upon doping and dedoping (oxidation and reduction for p-type materials, respectively) are likely to enable various applications. Some might be ideal for the design of electrochemical cells that maintain the same mechanical compliance during operation. An example is an OMIEC whose elastic modulus matches that of a specific type of cell culture or biological tissue throughout a complete oxidation/reduction cycle. This is because many cell cultures and tissues show a preference for substrates with lower elastic modulus,[55, 56] In contrast, some applications may require the opposite effect, a significant increase or decrease of the elastic modulus occurs during redox cycling. Despite its importance, the evolution of elastic modulus during redox cycling remains largely unexplored, highlighting the need for new device platforms to quantify these changes.[16]

Electrochemical doping of conjugated polymers, as briefly mentioned before, refers to the oxidation via electron transfer to or from a working electrode (WE). The resulting charges on the polymer backbone are compensated by the uptake of ions and solvent molecules from an electrolyte that is in contact with a reference electrode (RE) and/or counter electrode (CE) depending if it is a two or three electrode setup and dedoping is the opposite process, where the polymer goes back to the initial state. A three-electrode setup includes a WE, a CE and a RE The RE provides stable potential for accurate control of the WE, while the CE closes the circuit. (Figure 12c). The degree of electrochemical doping can be altered, or even reversed, by changing the potential that is applied at the WE, affecting the number of electrons transferred (mechanical properties depend not only on microstructural changes and counterions interactions but also on solvent interactions), in a two-electrode setup the CE is simultaneously serving as both reference and counter. The speed of electrochemical doping is governed by the drift of ions into the swollen polymer. The accompanied uptake/expulsion of ions and solvent

molecules leads to changes in the volume of the polymer, which is required for some applications like actuators and artificial muscles.[57]

3.1 How do electrochemical redox processes affect stiffness?

The ingression of solvated ions expands the polymer while the oxidation/reduction of the polymer backbone typically alters the nanostructure. More hydrophilic materials such as polythiophenes with oligoether side chains can take up not only ions but also solvent molecules. The amount of solvent that is taken up depends mainly on the anion size, electrolyte type, molarity and ionic strength.[16] This happens even in the absence of an applied electric field, which is known as passive swelling. As a result of the increase in volume, ion conduction pathways are created, i.e. the electrolyte is in contact with the conjugated polymer throughout its entire volume. This facilitates the ingression of ions and hence oxidation/reduction of the whole film once an electrochemical potential is applied. This is referred to as active swelling. In the case of an initially neutral polymer, charges are introduced to the polymer backbone, compensated by counterions that ingress from the electrolyte to balance the generated charges.

Electrochemical doping changes the nanostructure of conjugated polymers. Swelling of the polymer and oxidation/reduction of the backbone can lead to enhanced (or reduced) π-stacking and expansion of the lamellar stacking. This can shift the overall order of the conjugated polymers. These structural changes directly affect the polymer's elastic modulus (Figure 11), including (1) Plasticization, where counterions and especially solvent molecules soften the material. (2) Chain stiffening, where oxidation can make the polymer backbone more rigid and possibly accompanied by a change in ordering. (3) Ionic crosslinking, between counterions and oxidized polymer chains, which leads to an increase of stiffness. (4) Swelling, caused by the uptake of counterions and solvent molecules.[58]

These effects often have opposed effects and the balance between these determines the modulus during electrochemical doping and dedoping. For example, a polymer that takes up counterions but repels solvent molecules may show an invariant or even an increase in elastic modulus (ionic crosslinking outweighs plasticization). Conversely, if the solvent uptake is high there is an increased swelling and as a result a decrease in stiffness is likely expected.[59, 60]

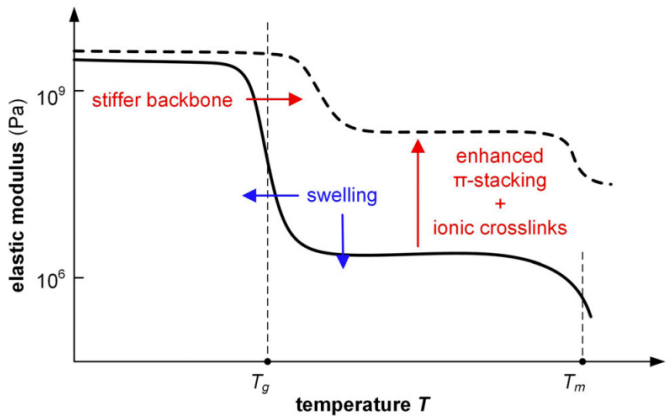

Figure 11. Dynamic mechanical analysis graph where the elastic modulus of a conjugated polymer can change upon doping due to the stiffening of the backbone, enhanced π-stacking, the formation of ionic crosslinks through polaron-counterions interactions and swelling because of the uptake of counterions and/or solvent molecules. Figure taken from [61].

3.2 Mechanical characterization techniques

Conjugated polymers are used for a wide range of applications, from thin film to bulk devices, each of which has its own requirements with respect to the mechanical properties of the polymers. The elastic modulus of conjugated polymer films under electrochemical doping and dedoping can be quantified with two complementary techniques: EC-AFM and EC-nanoindentation. Both are force microscopy techniques that facilitate the evaluation of the local mechanical properties of a sample. This is achieved by probing the elastic modulus of films immersed in an electrolyte during electrochemical doping and dedoping. This is achieved by recording force-displacement curves as a function of position. In AFM measured the repulsive force between the film surface and the cantilever tip, is determined by fitting the force curves, whereas nanoindentation measures the response of a polymer film to indentation by an indenter tip.[62] With nanoindentation creep analysis was used to obtain the elastic modulus. This consists of a three-segment protocol consisting of (1) a loading phase during which the applied load was gradually increased, (2) a hold phase where a constant load was maintained and (3) an unloading phase during which the tip was retracted (Figure 12a). Creep analysis analyzes gradual deformation of the film during the hold segment, since the deformation is time dependent. AFM, unlike nanoindentation, only accesses the linear (elastic) deformation regime since the interaction between the AFM tip and sample surface occurs through adhesive/repulsive forces

rather than prolonged contact (Figure 12b). Another difference between both techniques, which are limited by the setups, is that EC-nanoindentation works well in the micrometer thick film range while EC-AFM is used for nanometer thick films allowing to study the differences between the nanometer and micrometer thicknesses.

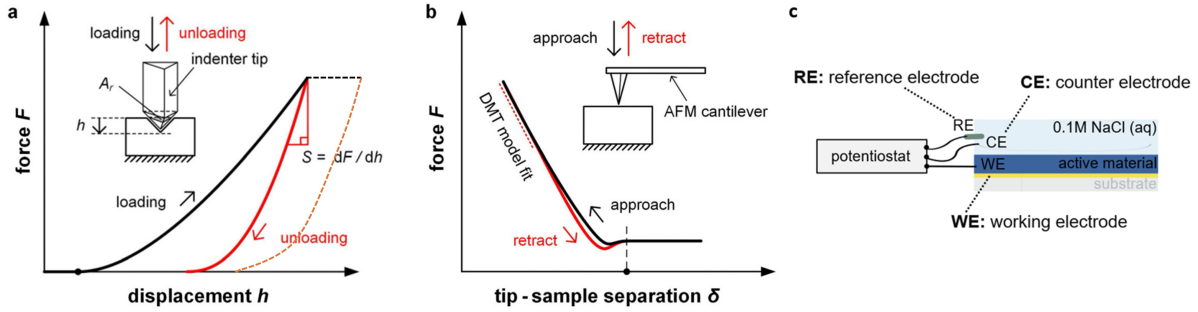

Figure 12. Force microscopy techniques. (a) Nanoindentation involves indentation of a polymer film with an indenter tip, followed by recording the unloading force curve from which the stiffness *S* can be determined; and (b) atomic force microscopy (AFM) can be used to measure the repulsive force between the cantilever tip and film surface, which can be fitted with the Derjaguin-Muller-Toporov (DMT) model. (c) 3 Electrode setup used to oxidize (dope) and reduce (dedope) the (WE is our polymer, RE is a silver/silver chloride (Ag/AgCl) electrode and CE is a platinum (Pt) wire). Figure a and b taken from paper [61].

3.2.1 Electrochemical nanoindentation

Measurements were performed at room temperature with a Hysitron TI Premier instrument from Bruker equipped with a Berkovich tip made of diamond with a half angle of α = 65.27° and a tip radius of 100 nm attached to a liquid compatible stylus, calibrated with a reference quartz substrate. Prior to each measurement, the nanoindenter was left in idle condition for half an hour to reach thermal equilibrium. The creep compliance was determined by recording the change in indentation depth $h(t)$ during the hold phase at a constant load of P_{hold} according to:[63]

$$J(t) = \frac{4h^2(t)}{\pi(1-\upsilon)\cdot P_{hold}\cdot \tan\alpha} \quad (1)$$

where υ = 0.35 is the Poisson ratio. The shear and tensile relaxation modulus, G and E, were calculated according to:

$$G = \frac{1}{J(t)}\Big|_{t \gg 0} \quad (2)$$

and

$$E = 3G \cdot (1 + \upsilon) \quad (3)$$

Reported values for E are the mean and standard deviation based on 9 to 12 creep measurements carried out using a loading rate of 20 μN s^{-1}, a maximum load varying from P_{hold} = 80 to 1000 μN and a hold time of 600 s.

Measurements of dry films without any electrolyte were carried out at 20% relative humidity. EC-NI was done by covering films with 0.1 M NaCl aqueous electrolyte contained in a reservoir defined by a 5 mm high polydimethylsiloxane (PDMS) well to which a 15 mL electrochemical cell was attached for oxidation or reduction at +0.6 V and -0.4 V vs. Ag/AgCl, respectively, in three-electrode configuration (Ag/AgCl reference electrode with 3 M KCl, Pt wire counter electrode and ITO or Au working electrode below the polymer film) using a SP-300 electrochemical workstation from BioLogic. Then, the sample and electrolyte reservoir (without the electrochemical cell) were transferred to the nanoindenter for EC-nanoindentation measurements. To maintain the same potential throughout the measurements an open circuit voltage V_{oc} was applied via a pseudo-reference Ag wire electrode embedded in the PDMS spacer with $V_{oc} = E_{Ag\ wire} - E_{Ag/AgCl}$ = 0.6 V – 0.52 V = 0.08 V (Figure 13).

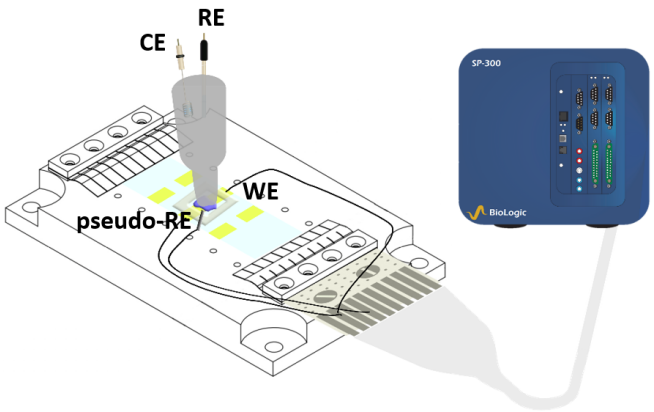

Figure 13. EC-nanoindentation three-electrode setup. Ag/AgCl reference electrode and Ag wire as the pseudo-reference electrode. Indium tin oxide (ITO) with the polymer film on top as the working electrode and Pt wire as the counter electrode.

Different materials were measured with nanoindentation under neat (dry) conditions, a good example is the copolymers mentioned in **Paper II**: P0, P12, P35 and P59. Where P0 is PTTEG (Figure 14b) and P12, P35, P59 are the side chains with different percentages (Figure 14c)). The reference polymer (P0) featured a modulus of 220 ± 13 MPa, the elastic modulus of P12 was 170 ± 32 MPa, the highest modulus was featured by P35 with a value of 236 ± 44 MPa and P59 was 170 ± 18 MPa (Figure 14a). It was shown by Moro *et al*. that glycol side chains do not interdigitate as well as alkoxy chains, leading to a decreased tendency to form ordered assemblies, influencing the microstructure of these semiconducting polymers potentially decreasing their elastic modulus.[64] However, the modulus changes of the polymer depending on the side chains content are all quite similar leading to the claim that the side chain chemistry can be altered without affecting the mechanical properties.

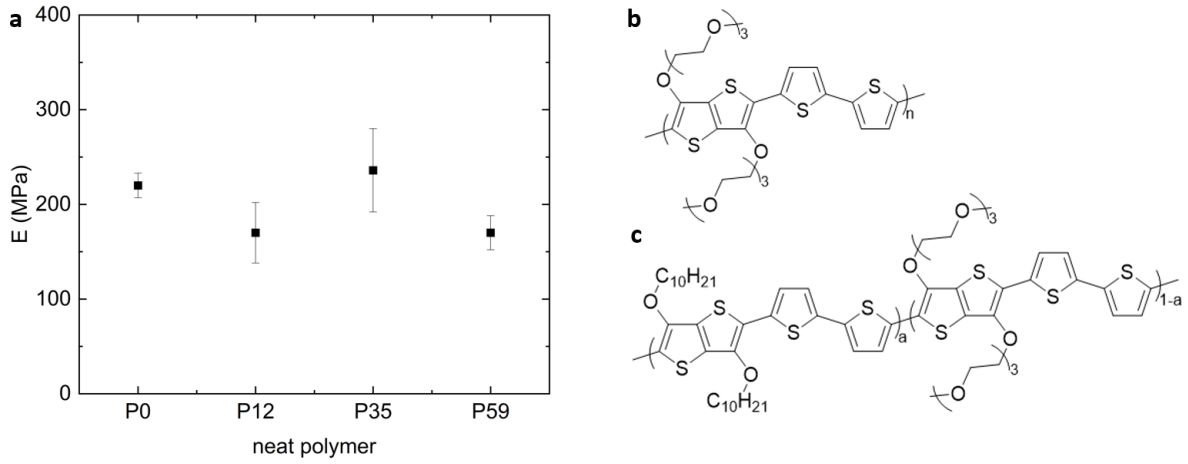

Figure 14. (a) Elastic modulus *E* obtained from nanoindentations from neat films. The overall mean is shown as a square and the standard deviation as error bars. (b) PTTEG (P0) and (c) general structure of PX, e.g., a = 0.12 for P12.

3.2.2 EC-AFM

EC-AFM was performed with a Dimension Icon XR from Bruker. The samples were mounted in an electrochemical cell filled with 0.1 M NaCl aqueous electrolyte, followed by sequential oxidation and reduction at +0.6 and -0.4 V vs. Ag/AgCl using a bipotentiostat and a three-electrode configuration (Pt wire counter electrode, Ag/AgCl pellet reference electrode and Au- working electrode below the polymer film). Measurements were performed by bringing the AFM probe in contact with the sample surface at a controlled load force of 5 nN and 100 force curves were recorded per sample/condition. Cycling reversibility was done the same way across seven redox cycles to confirm that the observed change in elastic modulus is reversible (Figure 15). The elastic modulus E was obtained by fitting force-distance curves $F(d)$ with a linearized model using the Nanoscope Analysis 2.0 software, assuming a Poisson's ratio υ = 0.35: (**Paper I)**

$$F = \frac{4}{3}\frac{E}{(1-\upsilon^2)}\sqrt{R}\,d^{3/2} \tag{4}$$

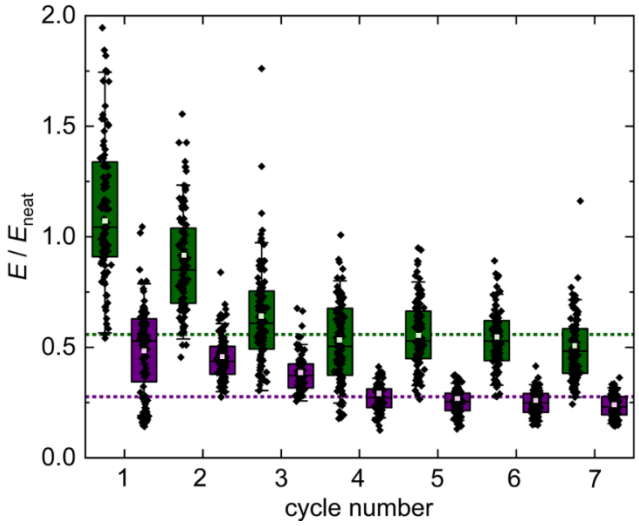

Figure 15. Changes in elastic modulus E for the same polymer covered by 0.1 M NaCl aqueous electrolyte upon repeated oxidation at +0.6 V (green) and reduction at -0.4 V vs. Ag/AgCl (purple) for 7 cycles, dashed lines represent the mean value of the last 5 cycles for the oxidized and reduced film, respectively.

3.2 Mechanical changes of PTTEG during electrochemical redox

As discussed previously, the mechanical response of conjugated polymers during redox cycling is still not well understood. Hence, it is important to determine how their stiffness evolves under different conditions. To establish a baseline, the reference material PTTEG (P0) was examined under four different conditions: (1) dry (neat) films, (2) passively swollen films submerged in 0.1 M NaCl (no bias), (3) films oxidized at +0.6 V vs. Ag/AgCl, and (4) films reduced at -0.4 V vs. Ag/AgCl (Figure 16a), along with the copolymers with different percentages of alkoxy/glycol side chains (Figure 16b).

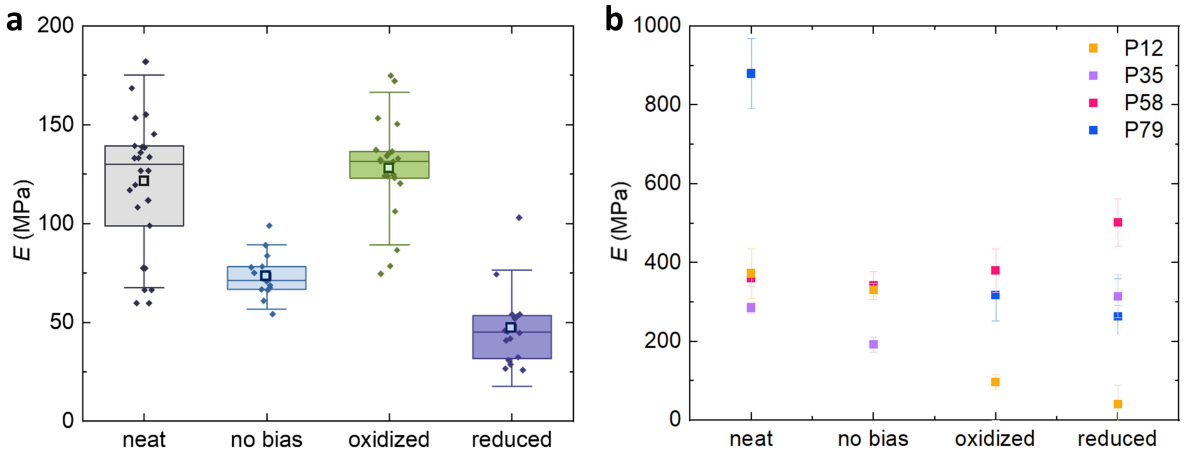

Figure 16. Elastic modulus *E* obtained from neat film measured without electrolyte (neat) and when covered by 0.1 M NaCl aqueous electrolyte, passive swelling (no bias), oxidized at +0.6 V or reduced at -0.4 V vs. Ag/AgCl for (a) PTTEG where each datapoint corresponds to the mean of values obtained from 9-12 creep measurements. The horizontal line inside each box indicates the median while the overall mean is shown as a square and the standard deviation as error bars and (b) the copolymers P12,35,58,79 where the square represents the mean with the corresponding standard deviation shown as error bars.

For PTTEG, the elastic modulus decreased with passive swelling (plasticization) and increased when oxidized – the swelling by the aqueous electrolyte is counteracted by a reversible improvement in π-stacking upon oxidation **(Paper II)**. Upon reduction the elastic modulus decreases going back to similar values as in the no bias (passive swelling). Here we used a diazirine PA (more information in **Paper I)** to avoid delamination during redox cycling. However, when we studied P12 to P79 we did not have the diazirine PA and as a result the delamination might have played an important role in the reading of the elastic modulus.

The findings in PTTEG demonstrate that it is feasible to design OMIEC materials with stable mechanical properties across redox states, opening new possibilities for compliant and tissue-matched bioelectronic interfaces that remain mechanically invariant during operation.

Chapter 4

Conclusions and outlook

This thesis has helped in a better understanding of OMIECs by studying a previously underexplored topics; the stability of materials in electrochemical devices as well as change of mechanical properties *in operando*. Using a thiophene-based copolymer system with different ratios of glycol and alkoxy side chains, the mechanical and electrical properties were studied upon redox cycling.

4.1 Conclusions

In this work, a reproducible step-by-step guide on how to fabricate OECTs has been explained, which will provide an improved learning platform as opposed to literature procedures which often lack extensive detail. This can be used as an SOP for students that want to start with OECT fabrication.

For the copolymer with variable side chains, an increase in oxidation onset potential was observed with the increase in alkoxy content, likely by hindering ion mobility and limiting charge compensation. Despite this, P12 and P35 achieve state-of-the-art maximum $[\mu C^*]_{max}$ values exceeding 1000 F cm^2 V^{-1} s^{-1}

This high performance is attributed to their combination of high mobility (μ) and high capacitance (C^*). However, the reason for poor capacitive behavior for P59 (alkoxy percentage $>$ 50%) requires further investigation.

Evaluation of material properties of PTTEG *in operando* reveals competition in structural changes during oxidation; swelling from uptake of hydrated ions and improved π-stacking in the polymer microstructure. This results in a small, reversible increase in elastic modulus upon electrochemical oxidation which differs from the assumption that ion and solvent uptake during swelling inherently results in material softening. Here, the microstructural changes outweigh the softening effects of solvent uptake. It is also shown that these changes are reversible and stable over many cycles which is essential for long term device reliability. Hence, probing that it is feasible to design OMIECs that maintain remarkably stable elastic moduli across redox states, opening new possibilities for compliant and tissue-matched bioelectronic interfaces that remain mechanically invariant during operation. Notwithstanding these results, *in operando*

techniques of mechanical property evaluation in electrochemical devices are now accessible, opening the way for deeper understanding of devices in operation essential for implementation in, e.g., living organisms.

OECT performance of these materials was characterized, and key figures of merit (μ, C*) were extracted using small signal analysis (SSA). Providing a way to compare electrical and mechanical properties.

4.2 Outlook

This work opens several directions for further research. Firstly, studying the mechanical properties of different copolymers without delamination (using diazirine PA) and extending that study to n-type and ambipolar OMIECs with different backbones and side chains, to build a comprehensive map of OMIECs (Ashby plot E vs μC^*). Secondly, how different electrolytes (ion size, polarity, concentration) impact the elastic modulus and its impact on swelling and microstructural ordering. This is ideally complemented with computational modelling which would predict electrochemical coupling based on chemicals structure, ionic mobility and solvent uptake. Moreover, it is clear from this work that the alteration between alkoxy and glycol side chains has little effect on the mechanical properties, meaning that these can be further implemented to achieve the best electrochemical performance and to control the tradeoffs between swelling and microstructural changes. Ultimately, this work will be an essential stepping stone for creating different devices with varying mechnical compliance; decoupling the electrical and mechanical changes during device operation.

ACKNOWLEDGEMENTS

This work is financially supported by the European Research Council (ERC) under grant agreement no. 101043417. The research presented in this thesis has been performed at the Division of Applied Chemistry and the Cleanroom Facilities at Chalmers.

The work presented in this thesis was not the result of just my efforts but rather a collaborative accomplishment shaped by the support, guidance, and encouragement of many people along the way. Hence, I would like to thank:

- My supervisor Christian Müller for guiding, supporting and mentoring me through these two years. It is rather rare to find a supervisor that busy that still makes as much time as you do for us. Your enthusiasm is contagious.
- All the current and former members of my working group. We are so lucky to be working together. I guess thanks again to Christian for choosing all of you. We are a big family where supporting, teaching and encouraging each other are our main values.
- All the people in the 8th floor, for being so welcoming. It is such a nice environment to work in (also always having lunch together). You make going to work something to be looking forward to. Thanks Lotta for taking care of all of us.
- Ruby and Emmy for being the best office mates, friends and workout partners. I never thought one could feel so loved and comfortable in an office. Mavi you were also key in that even if not in the same office. Meghna you could give energy to anyone, thanks for refilling my energy when it was low and Megan thanks for running at my pace I really enjoy our chatting runs. Joost thank you for always helping out (and also thanks for teaching me so much).
- Cristina, Sergi, Dedo, Marta, Blancas y Luisa por ser la mejor compañía y distracción.
- Alex, I cannot thank you enough. Thanks for your unconditional love and support. Of all the great things Sweden has given me, meeting you is by far the best.

Per últim, gràcies mama, papa i Nil per tot l'amor i suport que m'heu donat i per fer-me creure que puc aconseguir tot el que em proposi. Gràcies iaia Carmen, iaiona, avi Pepe i Eduard. Tinc la sort de ser una miqueta una suma de tots vosaltres. Us estimo.

BIBLIOGRAPHY

(1) Dickey, M. D. Stretchable and Soft Electronics using Liquid Metals. *Advanced Materials* **2017**, *29* (27). DOI: 10.1002/adma.201606425.

(2) Someya, T.; Bao, Z.; Malliaras, G. G. The rise of plastic bioelectronics. *Nature* **2016**, *540* (7633), 379-385. DOI: 10.1038/nature21004.

(3) Paulsen, B. D.; Tybrandt, K.; Stavrinidou, E.; Rivnay, J. Organic mixed ionic-electronic conductors. *Nature Materials* **2020**, *19* (1), 13-26. DOI: 10.1038/s41563-019-0435-z.

(4) Inal, S.; Malliaras, G. G.; Rivnay, J. Benchmarking organic mixed conductors for transistors. *Nature Communications* **2017**, *8* (1). DOI: 10.1038/s41467-017-01812-w.

(5) Rivnay, J.; Inal, S.; Salleo, A.; Owens, R. M.; Berggren, M.; Malliaras, G. G. Organic electrochemical transistors. *Nature Reviews Materials* **2018**, *3* (2), 17086. DOI: 10.1038/natrevmats.2017.86.

(6) Gkoupidenis, P.; Schaefer, N.; Garlan, B.; Malliaras, G. G. Neuromorphic Functions in PEDOT:PSS Organic Electrochemical Transistors. *Advanced Materials* **2015**, *27* (44), 7176-7180. DOI: 10.1002/adma.201503674 From NLM Medline.

(7) Lin, P.; Yan, F. Organic thin-film transistors for chemical and biological sensing. *Advanced Materials* **2012**, *24* (1), 34-51. DOI: 10.1002/adma.201103334 From NLM Medline.

(8) Khodagholy, D.; Gelinas, J. N.; Zhao, Z.; Yeh, M.; Long, M.; Greenlee, J. D.; Doyle, W.; Devinsky, O.; Buzsáki, G. Organic electronics for high-resolution electrocorticography of the human brain. *Science Advances* **2016**, *2* (11), e1601027. DOI: 10.1126/sciadv.1601027.

(9) Rivnay, J.; Owens, R. M.; Malliaras, G. G. The Rise of Organic Bioelectronics. *Chemistry of Materials* **2014**, *26* (1), 679-685. DOI: 10.1021/cm4022003.

(10) Oyaizu, K.; Nishide, H. Radical Polymers for Organic Electronic Devices: A Radical Departure from Conjugated Polymers? *Advanced Materials* **2009**, *21* (22), 2339-2344. DOI: 10.1002/adma.200803554.

(11) Yu, S.; Wu, H. Y.; Lemaur, V.; Kousseff, C. J.; Beljonne, D.; Fabiano, S.; Nielsen, C. B. Cation-Dependent Mixed Ionic-Electronic Transport in a Perylenediimide Small-Molecule Semiconductor. *Angewandte Chemie International Edition* **2024**. DOI: 10.1002/anie.202410626.

(12) Giovannitti, A.; Sbircea, D.-T.; Inal, S.; Nielsen, C. B.; Bandiello, E.; Hanifi, D. A.; Sessolo, M.; Malliaras, G. G.; McCulloch, I.; Rivnay, J. Controlling the mode of operation of

organic transistors through side-chain engineering. *Proceedings of the National Academy of Sciences* **2016**, *113* (43), 12017-12022. DOI: 10.1073/pnas.1608780113.

(13) Nielsen, C. B.; Giovannitti, A.; Sbircea, D.-T.; Bandiello, E.; Niazi, M. R.; Hanifi, D. A.; Sessolo, M.; Amassian, A.; Malliaras, G. G.; Rivnay, J.; et al. Molecular Design of Semiconducting Polymers for High-Performance Organic Electrochemical Transistors. *Journal of the American Chemical Society* **2016**, *138* (32), 10252-10259. DOI: 10.1021/jacs.6b05280.

(14) Stein, E.; Nahor, O.; Stolov, M.; Freger, V.; Petruta, I. M.; McCulloch, I.; Frey, G. L. Ambipolar blend-based organic electrochemical transistors and inverters. *Nature Communications* **2022**, *13* (1). DOI: 10.1038/s41467-022-33264-2.

(15) Friedlein, J. T.; McLeod, R. R.; Rivnay, J. Device physics of organic electrochemical transistors. *Organic Electronics* **2018**, *63*, 398-414. DOI: 10.1016/j.orgel.2018.09.010.

(16) Giovannitti, A.; Maria, I. P.; Hanifi, D.; Donahue, M. J.; Bryant, D.; Barth, K. J.; Makdah, B. E.; Savva, A.; Moia, D.; Zetek, M.; et al. The Role of the Side Chain on the Performance of N-type Conjugated Polymers in Aqueous Electrolytes. *Chemistry of Materials* **2018**, *30* (9), 2945-2953. DOI: 10.1021/acs.chemmater.8b00321.

(17) Amanchukwu, C. V.; Gauthier, M.; Batcho, T. P.; Symister, C.; Shao-Horn, Y.; D'Arcy, J. M.; Hammond, P. T. Evaluation and Stability of PEDOT Polymer Electrodes for Li–O₂ Batteries. *The Journal of Physical Chemistry Letters* **2016**, *7* (19), 3770-3775. DOI: 10.1021/acs.jpclett.6b01986.

(18) Argun, A. A.; Aubert, P.-H.; Thompson, B. C.; Schwendeman, I.; Gaupp, C. L.; Hwang, J.; Pinto, N. J.; Tanner, D. B.; Macdiarmid, A. G.; Reynolds, J. R. Multicolored Electrochromism in Polymers: Structures and Devices. *Chemistry of Materials* **2004**, *16* (23), 4401-4412. DOI: 10.1021/cm049669l.

(19) Lin, P.; Yan, F.; Yu, J.; Chan, H. L. W.; Yang, M. The Application of Organic Electrochemical Transistors in Cell-Based Biosensors. *Advanced Materials* **2010**, *22* (33), 3655-3660. DOI: 10.1002/adma.201000971.

(20) Malti, A.; Edberg, J.; Granberg, H.; Khan, Z. U.; Andreasen, J. W.; Liu, X.; Zhao, D.; Zhang, H.; Yao, Y.; Brill, J. W.; et al. An Organic Mixed Ion–Electron Conductor for Power Electronics. *Advanced Science* **2016**, *3* (2), 1500305. DOI: 10.1002/advs.201500305.

(21) Smela, E. Conjugated Polymer Actuators for Biomedical Applications. *Advanced Materials* **2003**, *15* (6), 481-494. DOI: 10.1002/adma.200390113.

(22) Ng, S. M. S. a. K. K. *Physics of Semiconductor Devices*; Wiley-Interscience, 2007.

(23) Facchetti, A. Semiconductors for organic transistors. *Materials Today* **2007**, *10* (3), 28-37. DOI: 10.1016/s1369-7021(07)70017-2.

(24) Khodagholy, D.; Rivnay, J.; Sessolo, M.; Gurfinkel, M.; Leleux, P.; Jimison, L. H.; Stavrinidou, E.; Herve, T.; Sanaur, S.; Owens, R. M.; et al. High transconductance organic electrochemical transistors. *Nature Communications* **2013**, *4* (1). DOI: 10.1038/ncomms3133.

(25) Rivnay, J.; Leleux, P.; Sessolo, M.; Khodagholy, D.; Hervé, T.; Fiocchi, M.; Malliaras, G. G. Organic Electrochemical Transistors with Maximum Transconductance at Zero Gate Bias. *Advanced Materials* **2013**, *25* (48), 7010-7014. DOI: 10.1002/adma.201303080.

(26) Rivnay, J.; Leleux, P.; Ferro, M.; Sessolo, M.; Williamson, A.; Koutsouras, D. A.; Khodagholy, D.; Ramuz, M.; Strakosas, X.; Owens, R. M.; et al. High-performance transistors for bioelectronics through tuning of channel thickness. *Science Advances* **2015**, *1* (4), e1400251. DOI: 10.1126/sciadv.1400251.

(27) Bernards, D. A.; Malliaras, G. G. Steady-State and Transient Behavior of Organic Electrochemical Transistors. *Advanced Functional Materials* **2007**, *17* (17), 3538-3544. DOI: 10.1002/adfm.200601239.

(28) Proctor, C. M.; Rivnay, J.; Malliaras, G. G. Understanding volumetric capacitance in conducting polymers. *Journal of Polymer Science Part B: Polymer Physics* **2016**, *54* (15), 1433-1436. DOI: 10.1002/polb.24038.

(29) Ortiz-Conde, A.; García-Sánchez, F. J.; Liou, J. J.; Cerdeira, A.; Estrada, M.; Yue, Y. A review of recent MOSFET threshold voltage extraction methods. *Microelectronics and reliability* **2002**, *42*, 583-596.

(30) Flagg, L. Q.; Bischak, C. G.; Onorato, J. W.; Rashid, R. B.; Luscombe, C. K.; Ginger, D. S. Polymer Crystallinity Controls Water Uptake in Glycol Side-Chain Polymer Organic Electrochemical Transistors. *Journal of the American Chemical Society* **2019**, *141* (10), 4345-4354. DOI: 10.1021/jacs.8b12640.

(31) Kumar Singh, V.; Mazhari, B. Measurement of threshold voltage in organic thin film transistors. *Applied Physics Letters* **2013**, *102* (25), 253304. DOI: 10.1063/1.4812191.

(32) Shahi, M.; Le, V. N.; Alarcon Espejo, P.; Alsufyani, M.; Kousseff, C. J.; McCulloch, I.; Paterson, A. F. The organic electrochemical transistor conundrum when reporting a mixed ionic–electronic transport figure of merit. *Nature Materials* **2024**, *23* (1), 2-8. DOI: 10.1038/s41563-023-01672-4.

(33) Kim, Y.; Kimpel, J.; Giovannitti, A.; Müller, C. Small signal analysis for the characterization of organic electrochemical transistors. *Nature Communications* **2024**, *15* (1). DOI: 10.1038/s41467-024-51883-9.
(34) Braendlein, M.; Lonjaret, T.; Leleux, P.; Badier, J. M.; Malliaras, G. G. Voltage Amplifier Based on Organic Electrochemical Transistor. *Advanced Science* **2017**, *4* (1), 1600247. DOI: 10.1002/advs.201600247.
(35) Campana, A.; Cramer, T.; Simon, D. T.; Berggren, M.; Biscarini, F. Electrocardiographic Recording with Conformable Organic Electrochemical Transistor Fabricated on Resorbable Bioscaffold. *Advanced Materials* **2014**, *26* (23), 3874-3878. DOI: 10.1002/adma.201400263.
(36) Leleux, P.; Rivnay, J.; Lonjaret, T.; Badier, J. M.; Bénar, C.; Hervé, T.; Chauvel, P.; Malliaras, G. G. Organic Electrochemical Transistors for Clinical Applications. *Advanced Healthcare Materials* **2015**, *4* (1), 142-147. DOI: 10.1002/adhm.201400356.
(37) Uguz, I.; Ganji, M.; Hama, A.; Tanaka, A.; Inal, S.; Youssef, A.; Owens, R. M.; Quilichini, P. P.; Ghestem, A.; Bernard, C.; et al. Autoclave Sterilization of PEDOT:PSS Electrophysiology Devices. *Advanced Healthcare Materials* **2016**, *5* (24), 3094-3098. DOI: 10.1002/adhm.201600870.
(38) Jimison, L. H.; Tria, S. A.; Khodagholy, D.; Gurfinkel, M.; Lanzarini, E.; Hama, A.; Malliaras, G. G.; Owens, R. M. Measurement of Barrier Tissue Integrity with an Organic Electrochemical Transistor. *Advanced Materials* **2012**, *24* (44), 5919-5923. DOI: 10.1002/adma.201202612.
(39) Ramuz, M.; Hama, A.; Rivnay, J.; Leleux, P.; Owens, R. M. Monitoring of cell layer coverage and differentiation with the organic electrochemical transistor. *Journal of Materials Chemistry B* **2015**, *3* (29), 5971-5977. DOI: 10.1039/c5tb00922g.
(40) Rivnay, J.; Leleux, P.; Hama, A.; Ramuz, M.; Huerta, M.; Malliaras, G. G.; Owens, R. M. Using white noise to gate organic transistors for dynamic monitoring of cultured cell layers. *Scientific Reports* **2015**, *5* (1), 11613. DOI: 10.1038/srep11613.
(41) Yao, C.; Xie, C.; Lin, P.; Yan, F.; Huang, P.; Hsing, I. M. Organic Electrochemical Transistor Array for Recording Transepithelial Ion Transport of Human Airway Epithelial Cells. *Advanced Materials* **2013**, *25* (45), 6575-6580. DOI: 10.1002/adma.201302615.
(42) Zhang, Y.; Inal, S.; Hsia, C. Y.; Ferro, M.; Ferro, M.; Daniel, S.; Owens, R. M. Supported Lipid Bilayer Assembly on PEDOT:PSS Films and Transistors. *Advanced Functional Materials* **2016**, *26* (40), 7304-7313. DOI: 10.1002/adfm.201602123.

(43) Bernards, D. A.; Macaya, D. J.; Nikolou, M.; Defranco, J. A.; Takamatsu, S.; Malliaras, G. G. Enzymatic sensing with organic electrochemical transistors. *J. Mater. Chem.* **2008**, *18* (1), 116-120. DOI: 10.1039/b713122d.

(44) Liao, C.; Zhang, M.; Niu, L.; Zheng, Z.; Yan, F. Highly selective and sensitive glucose sensors based on organic electrochemical transistors with graphene-modified gate electrodes. *Journal of Materials Chemistry B* **2013**, *1* (31), 3820. DOI: 10.1039/c3tb20451k.

(45) Pappa, A. M.; Curto, V. F.; Braendlein, M.; Strakosas, X.; Donahue, M. J.; Fiocchi, M.; Malliaras, G. G.; Owens, R. M. Organic Transistor Arrays Integrated with Finger-Powered Microfluidics for Multianalyte Saliva Testing. *Advanced Healthcare Materials* **2016**, *5* (17), 2295-2302. DOI: 10.1002/adhm.201600494.

(46) Tang, H.; Yan, F.; Lin, P.; Xu, J.; Chan, H. L. W. Highly Sensitive Glucose Biosensors Based on Organic Electrochemical Transistors Using Platinum Gate Electrodes Modified with Enzyme and Nanomaterials. *Advanced Functional Materials* **2011**, *21* (12), 2264-2272. DOI: 10.1002/adfm.201002117.

(47) Yang, S. Y.; Defranco, J. A.; Sylvester, Y. A.; Gobert, T. J.; Macaya, D. J.; Owens, R. M.; Malliaras, G. G. Integration of a surface-directed microfluidic system with an organic electrochemical transistor array for multi-analyte biosensors. *Lab Chip* **2009**, *9* (5), 704-708. DOI: 10.1039/b811606g.

(48) Andersson, P.; Forchheimer, R.; Tehrani, P.; Berggren, M. Printable All-Organic Electrochromic Active-Matrix Displays. *Advanced Functional Materials* **2007**, *17* (16), 3074-3082. DOI: 10.1002/adfm.200601241.

(49) Gualandi, I.; Marzocchi, M.; Achilli, A.; Cavedale, D.; Bonfiglio, A.; Fraboni, B. Textile Organic Electrochemical Transistors as a Platform for Wearable Biosensors. *Scientific Reports* **2016**, *6* (1), 33637. DOI: 10.1038/srep33637.

(50) Hamedi, M.; Forchheimer, R.; Inganäs, O. Towards woven logic from organic electronic fibres. *Nature Materials* **2007**, *6* (5), 357-362. DOI: 10.1038/nmat1884.

(51) Nilsson, D.; Robinson, N.; Berggren, M.; Forchheimer, R. Electrochemical Logic Circuits. *Advanced Materials* **2005**, *17* (3), 353-358. DOI: 10.1002/adma.200401273.

(52) Emelyanov, A. V.; Lapkin, D. A.; Demin, V. A.; Erokhin, V. V.; Battistoni, S.; Baldi, G.; Dimonte, A.; Korovin, A. N.; Iannotta, S.; Kashkarov, P. K.; et al. First steps towards the realization of a double layer perceptron based on organic memristive devices. *AIP Advances* **2016**, *6* (11), 111301. DOI: 10.1063/1.4966257.

(53) Gkoupidenis, P.; Koutsouras, D. A.; Malliaras, G. G. Neuromorphic device architectures with global connectivity through electrolyte gating. *Nature Communications* **2017**, *8* (1), 15448. DOI: 10.1038/ncomms15448.

(54) Xu, W.; Min, S.-Y.; Hwang, H.; Lee, T.-W. Organic core-sheath nanowire artificial synapses with femtojoule energy consumption. *Science Advances* **2016**, *2* (6), e1501326. DOI: 10.1126/sciadv.1501326.

(55) Guo, A.; Wang, B.; Lyu, C.; Li, W.; Wu, Y.; Zhu, L.; Bi, R.; Huang, C.; Li, J. J.; Du, Y. Consistent apparent Young's modulus of human embryonic stem cells and derived cell types stabilized by substrate stiffness regulation promotes lineage specificity maintenance. *Cell Regeneration* **2020**, *9* (1). DOI: 10.1186/s13619-020-00054-4.

(56) Lv, H.; Li, L.; Sun, M.; Zhang, Y.; Chen, L.; Rong, Y.; Li, Y. Mechanism of regulation of stem cell differentiation by matrix stiffness. *Stem Cell Research & Therapy* **2015**, *6* (1). DOI: 10.1186/s13287-015-0083-4.

(57) Jager, E. W. H.; Smela, E.; InganäS, O. Microfabricating Conjugated Polymer Actuators. *Science* **2000**, *290* (5496), 1540-1545. DOI: 10.1126/science.290.5496.1540.

(58) Keng, Y.; Pillai, P. V.; Hunter, I. W. The Effect of Ion Delivery on Polypyrrole Strain and Strain Rate under Elevated Temperature. *MRS Proceedings* **2009**, *1222*. DOI: 10.1557/proc-1222-dd02-10.

(59) Savva, A.; Cendra, C.; Giugni, A.; Torre, B.; Surgailis, J.; Ohayon, D.; Giovannitti, A.; McCulloch, I.; Di Fabrizio, E.; Salleo, A.; et al. Influence of Water on the Performance of Organic Electrochemical Transistors. *Chemistry of Materials* **2019**, *31* (3), 927-937. DOI: 10.1021/acs.chemmater.8b04335.

(60) Stavrinidou, E.; Gabrielsson, R.; Gomez, E.; Crispin, X.; Nilsson, O.; Simon, D. T.; Berggren, M. Electronic plants. *Science Advances* **2015**, *1* (10), e1501136. DOI: 10.1126/sciadv.1501136.

(61) Paleti, S. H. K.; Kim, Y.; Kimpel, J.; Craighero, M.; Haraguchi, S.; Müller, C. Impact of doping on the mechanical properties of conjugated polymers. *Chemical Society Reviews* **2024**, *53* (4), 1702-1729. DOI: 10.1039/d3cs00833a.

(62) Chen, X.; Li, B.; Liao, Z.; Li, J.; Li, X.; Yin, J.; Guo, W. Principles and Applications of Liquid-Environment Atomic Force Microscopy. *Advanced Materials Interfaces* **2022**, *9* (35), 2201864. DOI: 10.1002/admi.202201864.

(63) Paleti, S. H. K.; Haraguchi, S.; Cao, Z.; Craighero, M.; Kimpel, J.; Zeng, Z.; Sowinski, P.; Zhu, D.; Pons, I. T. J.; Kim, Y.; et al. Benchmarking the Elastic Modulus of Conjugated

Polymers with Nanoindentation. *Macromol* **2025**, *58* (7), 3578-3588. DOI: 10.1021/acs.macromol.4c03081.

(64) Moro, S.; Siemons, N.; Drury, O.; Warr, D. A.; Moriarty, T. A.; Perdigão, L. M. A.; Pearce, D.; Moser, M.; Hallani, R. K.; Parker, J.; et al. The Effect of Glycol Side Chains on the Assembly and Microstructure of Conjugated Polymers. *ACS Nano* **2022**, *16* (12), 21303-21314. DOI: 10.1021/acsnano.2c09464.